J. Sustain. Metall. (2015) 1:199–215
DOI 10.1007/s40831-015-0021-9

RESEARCH ARTICLE

Recycling of NdFeB Magnets Using Sulfation, Selective Roasting, and Water Leaching

Mehmet Ali Recai Önal[1] · Chenna Rao Borra[2] · Muxing Guo[1] · Bart Blanpain[1] · Tom Van Gerven[2]

Published online: 7 July 2015

Abstract NdFeB magnets currently dominate the magnet market. Supply risks of certain rare earth metals (REMs), e.g., Nd and Dy, demand efficient recycling options that are applicable to different types and compositions with minimum use of chemicals and waste generation. In this study, a hydrometallurgical method is presented, which is adjustable to all NdFeB magnets, regardless of their composition. After completely transforming powdered samples into a sulfate mixture, a suitable selective roasting and water leaching treatment resulted in 95–100 % extraction efficiencies for Nd, Dy, Pr, Gd, Tb, and Eu, while Fe remained in the resultant residue forming a marketable hematite-dominated by-product. Impurities other than Fe were also greatly separated from the leachate thereby enabling the production of a liquid with at least 98 % REM purity. Such a solution then can be directly treated with subsequent shortened downstream processes without pretreatments for impurity removal. Due to decomposition reactions of impurities, including Fe, during the selective roasting stage, the majority of consumed acid is recyclable resulting in an environment-friendly flow sheet.

Keywords Recycling · NdFeB magnets · Sulfation · Roasting · Water leaching

The contributing editor for this article was Yiannis Pontikes.

✉ Mehmet Ali Recai Önal
mehmetalirecai.onal@mtm.kuleuven.be

[1] Department of Materials Engineering, KU Leuven, Kasteelpark Arenberg 44, 3001 Leuven, Belgium

[2] Process Engineering for Sustainable Systems (ProcESS), Department of Chemical Engineering, KU Leuven, De Croylaan 46, 3001 Leuven, Belgium

Introduction

Currently, the strongest magnets available belong to the NdFeB magnet family [1]. NdFeB magnets are composed of 30–40 wt% rare earth metals (REMs) (15–30 wt% of which is Nd) and 60–70 wt% other elements (50–70 wt% of which is Fe along with ~1 wt% B). Alterations to the composition can occur due to required operating temperature and medium, availability of the constituents, admixtures, and manufacturer. As for Dy, it can vary from close to 0 wt% (hard disk drives, HDDs) to as high as 8.5 wt% (electric car motors) [2]. Other REMs (Pr, Tb, Gd, Eu) or other elements such as Al, Co, Ga, Nb, Ni, Si, Zn, etc., can also be used as minor admixtures or coating material for improving the thermal and oxidation–corrosion resistances of the magnets [3–6].

In 2008, NdFeB magnets accounted for 21 % of all REM consumption by volume, and the highest growth rate of REM applications was expected from these magnets [7]. Considering the expected increase in demands for Nd and Dy in the next 25 years, the progressive cut in China's REM export quota in 2009 showed how their monopoly can endanger the supply chain for NdFeB magnets [2, 8]. Recycling of NdFeB magnets has become one of the few solutions for this problem. While pre-consumer scraps are by and large recycled internally as in Hitachi metals [9], for end-of-life (EOL) scraps, recycling is far from pervasive due to lack of strategies for collecting and dismantling of the magnet part [10–13]. Recently, a patented study offered a promising solution to facilitate separation of EOL magnets by hydrogen decrepitation (HD) [14]. However, the applicability of HD on different composition blends (i.e., higher Dy wt%) and O contents is currently unknown as HDD magnets are covered with a protective Ni coating that minimizes the oxidation and have minor admixtures.

The same EOL scraps can be directly re-used by demagnetization and re-magnetization to produce the same magnets for the same products [15, 16]. Even though this is clearly the best recycling option, it is applicable only if the waste magnet is well conserved and uncontaminated. However, such scraps are not available in large quantities [2]. In the other case, a processing route is necessary to achieve recycling. Several innovative attempts to recycle different types of magnet scraps have been reported in the literature [2, 15, 17, 18]. These attempts were critically evaluated elsewhere [2]; nonetheless, we can indicate here that hydrometallurgical methods form the basis of the conventional recycling flow sheet. This is most probably because they can be easily adjusted to REM ore-processing industry where hydrometallurgical flow sheets are dominant [19]. For instance, an acid leaching process can produce a fairly concentrated and marketable leachate that can be processed in any operating REM separation plant [15].

Either whole acid leaching [20–22] or selective acid leaching [9, 23–25] option has been studied so far. In whole leaching, the acid consumption is high and, by definition, there is no selectivity for REM at all, which is why selective precipitation is the common next step [26]. In order to improve selectivity, oxidation roasting is applied on scrap, and acid leaching is followed by solvent extraction (SX). Magnet scrap is oxidized in air between 500 °C [23] and 950 °C [9] for up to 15 h, depending on the particle size and the composition of the magnet as well as the desired microstructure of the oxidized product. The major aim is to ensure that any dissolved iron will be in the form of Fe^{3+}, which is less stable than Fe^{2+}. This way, selectivity is improved since during leaching at a pH above 2–3, Fe^{3+} will precipitate, while REMs will remain in solution. However, extraction efficiencies of metals are related to several parameters. Formation of Nd–Fe oxide complexes like $NdFeO_3$ should be avoided during oxidation as it suppresses Nd extraction [24]. Any unoxidized iron will dissolve during leaching and remain in the solution as Fe^{2+} up to pH values of 6–8. Hence, too much oxidation will result in poor REM extraction, whereas insufficient roasting will cause poor selectivity because of Fe^{2+} dissolution. Also, impurities other than Fe and their oxides dissolve into solution with sufficient acid addition, usually forming stabler cations than Fe^{3+}. This means that even with selective leaching, a certain amount of impurities will contaminate the leachate, and their removal in subsequent SX will still be required. This will complicate and expand the flow sheet [9, 15, 27].

The purpose of this study is to transform the whole magnet material into sulfates by digestion in concentrated sulfuric acid at ambient temperature. When this transformation is complete, the mixture is selectively roasted to obtain a calcine containing water-soluble REM-sulfates and water-insoluble impurity-oxides. By leaching this calcine with water at ambient conditions, it is possible to extract all existing REMs into a slightly acidic leachate (pH 5) leaving behind the impurity-oxides in the solid residue. This study offers a simple and controllable processing alternative that is completely compatible with the already existing REM-ore-processing plants [19].

Theoretical Background

Chemistry of Sulfuric Acid Mixing

During acid mixing of the magnet, the reactions between sulfuric acid and metals result in the formation of metal sulfates. Most of the metals including REMs readily react with dilute acid by replacing hydronium ions giving the net reaction (1), where M is metal. However, metals below hydrogen in the electropotential series (e.g., Cu) do not respond to the dilute sulfuric acid attack. In contrast, concentrated H_2SO_4 can also act as a strong oxidizing agent. Hence, it can react with the metals, even those under hydrogen, where the reaction by-products are now water vapor and SO_2 gas. Here, S in the acid is reduced and partially leaves the system in gaseous state enabling metal sulfate formation by the net reaction (2).

$$x\ M + y\ H_2SO_{4(aq)} \rightarrow M_x(SO_4)_{y(aq)} + y\ H_{2(g)} \quad (1)$$

$$x\ M + 2y\ H_2SO_{4(aq)} \rightarrow M_x(SO_4)_y(aq) + 2y\ H_2O_{(g)} + y\ SO_{2(g)} \quad (2)$$

Although it contains more moles of protons than dilute acid in the same volume, concentrated sulfuric acid is somewhat less reactive on metals, more importantly on REMs [28]. This is most probably associated with the formation of a protective oxide/sulfate interface between metal and acid slowing down or inhibiting the reaction depending on the stability of the layer. Due to its fairly high boiling point, with supplied heat, reaction kinetics is enhanced, and the protective layer is forced to dissolve or simply fall off within sufficient time.

Thermal Decomposition and Water Solubility of Metal Sulfates

Selective roasting is the most crucial step in this study, and it is based on differences in thermal decomposition of metal sulfates, which result from the reactions between sulfuric acid and metals of the NdFeB magnets. These metals are REMs, Fe, Al, Co, Nb, Ga, Cu, Mn, Ni, and Zn.

The thermodynamic stability of most of the considered metal sulfates are listed in increasing order [29]:

$$Al_2(SO_4)_3 < Fe_2(SO_4)_3 < CuSO_4 < ZnSO_4 < NiSO_4 < CoSO_4 < La_2(SO_4)_3 < MnSO_4$$

Hence, with an appropriate selective roasting treatment, it is possible to transform the sulfates of almost all impurity metals into their respective oxides while REMs (e.g., La) remain in their sulfate form. However, the relative stability of metal sulfates cannot be predicted solely by thermodynamic data. It should also be noted that the thermal stability of any metal sulfate is also dependent on other factors (e.g., heating rate) that could shift its decomposition range from the reported cases. These factors are listed in detail elsewhere [30–32].

Thermal Decomposition and Water Solubility of REM Sulfates

Wendlandt and George [30] reported that hydrated sulfates of all heavy REMs including Eu through Lu (except Yb) experience 2-step dehydration: from octahydrate to dihydrate and then to anhydrous sulfate before 300 °C. On the other hand, the sulfates of Yb and light REMs (La through Sm) experience three-step dehydration: from octa/nonahydrate to pentahydrate, from pentahydrate to dihydrate, and finally to anhydrous sulfate before 350 °C [30]. Further increases in temperature give a stepwise decomposition of anhydrous sulfates by reactions (3–4) where R is REM.

$$R_2(SO_4)_3 \rightarrow R_2O_2(SO_4) + 2\ SO_{3(g)} \quad (3)$$

$$R_2O_2(SO_4) \rightarrow R_2O_3 + SO_{3(g)} \quad (4)$$

Formation of an intermediate oxysulfate is common for all REM (III) sulfates. Water solubility of oxysulfates is only partial, but they are fully soluble in dilute acids [33]. The water solubility of REM sulfates is given in Table 1 [34, 35]. The solubility of their oxysulfates, however, can be considered as negligible [36]. The end product of thermal decomposition is usually an oxide of R_2O_3 form. The oxides of REMs as well as of many other metals are practically insoluble in water with few exceptions like B_2O_3 [37]. Within the scope of this study, the decomposition temperatures given for reaction (3) are more important than for reaction (4). This is because these temperatures imply the maximum temperature for a selective roasting action in which the considered REMs are conserved as water-soluble anhydrous sulfates.

The stability of REM sulfates decreases in the order of La–Y–Lu–Pr–Nd–Sm–Eu but then increases in the order of Tb–Dy–Ho–Er–Tm–Yb. It then drops to a moderate level for Gd and significantly decreases through Sc–Ce(III)–Ce(IV) [38, 39]. Nathans and Wendlandt gave 855–946 °C as the temperature range for reaction (3) to be noticeable (except Ce and Sc) under inert atmosphere [40]. The decomposition temperatures or ranges from three studies are listed in Table 2 [38, 40, 41]. These results were partially confirmed by contemporary studies. Tomaszewicz et al. reported onset temperature for transformation of $Gd_2(SO_4)_3$ to $Gd_2O_2(SO_4)$ to be 983 °C in inert and 1000 °C in oxidizing atmosphere with 10 °C/min heating rate [42]. Poston et al. reported a dramatic weight loss at 800 °C and a moderate loss until 890 °C representing the decomposition of $Sm_2(SO_4)_3$ to give $Sm_2O_2(SO_4)$ at 5 °C/min heating rate under inert atmosphere [32]. Although Sm is not observed in NdFeB magnets, in case of a blend of SmCo and NdFeB magnet scraps subjected to this study, the maximum temperature of roasting would be determined by the thermal decomposition behavior of Sm-sulfate so as to completely dissolve Sm in water.

Thermal Decomposition of Iron Sulfates

Since iron constitutes 50–70 wt% of a typical NdFeB magnet composition, selectivity against Fe is the major goal of any recycling study. Hence, the thermal decomposition behavior of iron sulfates is of great interest here. Depending on the original oxidation state, ferrous ($FeSO_4$) or ferric ($Fe_2(SO_4)_3$) sulfates can be formed. Leaching of unoxidized NdFeB magnets in dilute sulfuric acid produces ferrous ion into solution by reaction (1). Both sulfates have

Table 1 Water solubility of selected compounds

Compound	Solubility (g/100 g of H_2O)/temperature (°C)							
	$Nd_2(SO_4)_3.8H_2O$	$Pr_2(SO_4)_3.8H_2O$	$Dy_2(SO_4)_3.8H_2O$	$Gd_2(SO_4)_3.8H_2O$	$Tb_2(SO_4)_3.8H_2O$	$Eu_2(SO_4)_3.8H_2O$	$Sm_2(SO_4)_3.8H_2O$	$FeSO_4.7H_2O$
Kaye and Laby [34]	7.1/20–1.2/100	12.6/20–1.0/96	4.1/20–2.7/40	2.3/20–1.8/40	2.9/20–2.0/40	2.1/20–1.8/40	3.5/25–1.6/40	26.3/20–34.2/95
Compound	$Fe_2(SO_4)_3{\cdot}9H_2O$	$Al_2(SO_4)_3$	$CoSO_4{\cdot}7H_2O$	$CuSO_4{\cdot}5H_2O$	$NiSO_4{\cdot}7H_2O$	B_2O_3	$MnSO_4{\cdot}4H_2O$	$ZnSO_4{\cdot}7H_2O$
Lide [35]	440/20	38.5/25	38.3/25	22.0/25	40.4/25	2.2/20	63.7/25	57.7/25

Table 2 Thermal decomposition temperatures or temperature ranges for several metal sulfates

Reference	Heating rate (°C/min)	Thermal decomposition temperature (°C)						
		$Dy_2(SO_4)_3$	$Gd_2(SO_4)_3$	$Nd_2(SO_4)_3$	$Pr_2(SO_4)_3$	$Tb_2(SO_4)_3$	$Eu_2(SO_4)_3$	$Sm_2(SO_4)_3$
Nathans and Wendlandt [40]	10	910-1140	1027	1027	1000	883-1090	870-1014	800
Wilfong et al. [41]	2.5	NA	NA	810-1000	800-1000	NA	NA	800-985
Stern [39]	NA	888-1069	858-1014	890-1060	910-1085	880-1047	NA	890-1040

Reference	Heating rate (°C/min)	$Al_2(SO_4)_3$	$CuSO_4$	$ZnSO_4$	$NiSO_4$	$CoSO_4$	$MnSO_4$
Habashi [33]	NA	590–640	650–710	700–780	700–765	720–770	700–800
Tagawa [43]	5	524	605	630	676	690	717
Collins et al. [44]	6	700–900	500–700	NA	NA	NA	NA
Kolta and Askar [45]	5	NA	625/655	675/682	675/678	720/722	NA
	NA		598, 600, 620, 624	610, 646, 675, 846	675, 730, 750, 848	550, 708, 730, 820, 904	
Siriwardane et al. [46]	5	NA	550–850	600–800	600–800	NA	NA

high solubility in water (Table 1) and similar decomposition schemes where the end product is always water-insoluble α-Fe_2O_3. According to Habashi, all sulfates behave similarly in both inert and oxidizing atmospheres except $FeSO_4$ which exhibits a complex thermal decomposition mechanism in oxidizing atmospheres [33].

Dehydration of $FeSO_4{\cdot}7H_2O$ into monohydrate is completed in the range of 130–200 °C. From that point, two different pathways were proposed for its decomposition under oxidizing atmosphere. In the first one, an intermediate oxysulfate ($Fe_2O(SO_4)_2$) is formed by simple dehydration and subsequent oxidation of the monohydrate. In the second and competing scheme, an intermediate basic sulfate ($FeOHSO_4$) is formed by direct oxidation of the monohydrate. In both cases, these intermediates finally decompose to hematite within 550–800 °C range [33, 47–50]. Galwey and Brown summarized a combination of these pathways where ferric sulfate formation was also included [51]. Accordingly, $FeSO_4.H_2O$ undergoes a concurrent oxidation and hydrolysis to form both of these intermediates where oxidation is completed at 345 °C. The intermediates subsequently transform to $Fe_2(SO_4)_3$, which further decomposes to give hematite. Siriwardane et al. found no weight loss in the monohydrate until around 500 °C although both $FeOHSO_4$ and $Fe_2S_2O_9{\cdot}xH_2O$ were identified at 300 °C by XRD analysis. With further heating, first only $Fe_2(SO_4)_3$ at 550 °C, and then only Fe_2O_3 at 600 °C was detected with no presence of any intermediate oxysulfate [46]. Stern and Weise and Stern reported that when $FeSO_4$ is heated above 550 °C, the decomposition product is FeO, but it immediately oxidizes to Fe_2O_3 by oxygen from air or from slow decomposition of SO_3 giving the net reaction (5) [38, 39].

$$2\ FeSO_4 \rightarrow 2\ Fe_2O_3 + SO_{2(g)} + SO_{3(g)} \quad (5)$$

The thermal decomposition behavior of $Fe_2(SO_4)_3$ is a straightforward process. It directly decomposes to give hematite by releasing SO_3 gas. Several authors reported different temperature ranges as: 500–600 °C and 550–625 °C [46], 500–545 °C [43], and 575–600 °C [45], but it is clear that its thermal decomposition is completed at around 600 °C. It should be noted for recycling purposes that the by-product gas mixture due to thermal decomposition of iron sulfates (and other metal sulfates) can be easily collected to reproduce the acid consumed by these metals during acid mixing stage (i.e., sulfation). In general, a closed loop for sulfur is possible, although an efficient and economic oxidation and adsorption of the off-gas for production of sulfuric acid needs to be found.

Thermal Decomposition of Other Metal Sulfates

Being present in minor amounts, other metals can also be considered as impurity, and their presence in the leachate can be important for the subsequent downstream processes. Thermal decomposition reactions of the considered metal sulfates can be classified as in [36] where SO_2 and/or SO_3 gases are by-products. The decomposition temperatures or ranges for Al, Cu, Zn, Ni, Co, and Mn sulfates are summarized in Table 2, which is based on previous reports [33,

43–46]. Kolta and Askar [45] reported results from both their own study (upper row: TG/DTA) and from earlier literature (lower row).

Although thermodynamically the least stable sulfate is expected to be $Al_2(SO_4)_3$, its decomposition behavior seems to be contradictory. $Ga_2(SO_4)_3$ is less stable than $Al_2(SO_4)_3$ and decomposes at 560–700 °C [38]. As agreed by the thermodynamic data, $NiSO_4$ is less stable than $CoSO_4$ where end products are Co_3O_4 and NiO for oxidizing atmospheres [39]. $CuSO_4$ and $ZnSO_4$ undergo two-step decomposition where intermediate oxysulfates of $CuO.CuSO_4$ and $ZnO{\cdot}ZnSO_4$ are formed initially to give end products of CuO and ZnO. No data could be found for thermal decomposition behavior of niobium sulfate, but it is known that metallic niobium can resist any concentrations of sulfuric acid up to 95 % at room temperature in oxidizing conditions [52].

Materials and Methods

Sample Preparation

All magnet samples used in this study were supplied by Magneti Ljubljana-D.D. (Slovenia) in bulk form. The samples were produced for the automotive industry, but failed visual standards and were rejected before magnetization. Hence, demagnetization was not required. The study was focused on the high grade (HG) sample, containing a relatively high Dy, Pr, and Gd content. Additional experiments were performed with Ni-coated (NC) and fully oxidized HG (FO) samples. Cylindrical (HG) or cubic (NC) magnet pieces were first ground in a disk mill (Benelux Scientific) and sieved to obtain <500 μm powders. These samples were then fed in a planetary ball mill (Retsch PM4000, 5 mm stainless steel balls) for further grinding to obtain <40, <125, and <200 μm samples. Ball milling conditions for the HG sample were 15:1–45:1 ball:powder ratio (g/g), 1–3-h duration, and 100–300 rpm to obtain different particle sizes. In order to prevent ignition during or after ball milling [9], the stainless steel pots were loaded under Ar atmosphere. For the NC sample, 5:1 ball:powder ratio (g/g), 1-h duration, and 100 rpm were used as processing conditions. These were less severe conditions than for the HG sample, because the Ni coating is more ductile and causes the powders to stick to the milling pot. Bulk and powder samples were stored in a desiccator filled with N_2 to prevent continuous and uncontrollable oxidization, and the inert atmosphere was refreshed each month. A HG sample with <40 μm size was intentionally fully oxidized in a box furnace at 650 °C for 4 h to obtain stabilized (33.7 %) weight gain.

Materials Characterization

Powder mineralogy was characterized by a Seifert 3003 T/T model X-ray diffractometer (XRD) with a Cu-Kα X-ray tube operated at 40 kV and 40 mA. Raw data were processed with the X'pert HighScore Plus PANalytical software. Chemical analysis of leachates was performed using a Varian 720 ES model inductively coupled plasma optical emission spectroscope (ICP-OES), while solid samples were analyzed using a Philips PW 2400 model wavelength dispersive X-ray fluorescence spectrometer (WD-XRF). In order to understand the responsible mechanism of valuable metal losses into the leach residue, a Philips XL30 FEG model scanning electron microscope (SEM) and JEOL JXA-8530F model electron probe microanalysis (EPMA) were used. Point analyses were taken with EPMA operated at 15 kV. Thermal decomposition behavior of dried acid–magnet mixture was analyzed by T.A. Instruments Q600 model SDT (simultaneous differential scanning calorimetry (DSC) and thermogravimetric analysis (TGA)) at 10 °C/min heating rate under 100 ml/min dry air flow. Due to its highly corrosive and hydrophilic nature, further tests on the dried acid–magnet mixture were not possible.

Experimental Set-Up and Procedure

12–16 M acid solutions were prepared by mixing 1.17–5.85 ml of 95–97 % sulfuric acid (Sigma-Aldrich, grade 30743) with 0.6–1.5 ml of demineralized water. 1 g or 2.5 g of powder sample was mixed in a cylindrical alumina crucible with the acid solutions by acid:magnet ratio (g/g) of 2.15 (12 M), 3.2 (13.5 M), 4.3 (14.5 M), and 8.6 (16 M). Additional experiments were performed at low acid concentrations (12 and 13.5 M) by simultaneously stirring the mixture with a silica fume glass rod. Once severe bubbling was achieved, random and rigid tablet-like formations at the bottom of the crucible were detected during the acid mixing stage. These tablets were gently disintegrated and bubbling continued as the acid–magnet reaction was not yet complete. The silica rod was then swiped with hardened ashless filter paper (Whatman grade 542) to recover all material before the drying step. None of these precautions were needed or applied for the higher acid concentrations although the same sintering problem was detected. The mixtures were dried in a muffle furnace under a fume hood at 110 °C for 6–24 h. The dried samples were then placed in the same furnace preheated to 650–850 °C for selective roasting for 15–120 min. The obtained calcines were quantitatively scraped off from the crucibles by a scraper and loaded into 50 ml PE plastic bottles along with 25–50 ml demineralized water. In order

to observe the weight change and make sure nothing was left in the crucibles, sample weights were measured after each step. Also, leaching water was passed through the crucibles before leaching experiments to ensure any water-soluble calcine material can pass to the system. This way, extraction efficiencies of metals are not affected. Bottles were placed on a unidirectional horizontal shaker, and the calcines were leached for 15 min to 24 h at 225 rpm. Solutions for analysis were obtained after leaching by filtering the sludge through a syringe filter with 0.45 μm pore size. Solid residues for XRD, XRF, SEM, and EPMA analyses were obtained by filtering the sludge under vacuum through a Buchner funnel with the Whatman-grade 542 filter paper. The filter cake was subsequently washed with ca. 500 ml demineralized water to completely remove any entrapped leachate and then dried overnight at 60 °C before analysis. After each filtration, the pH of the leachate was determined with a Pt–Ag/AgCl electrode that was saturated with 3 M KCl solution (WTW Sentix 81). The extraction efficiency of any metal M was calculated based on Eq. (6). The purity of the leachate is calculated based on Eq. (7).

$$\text{Extraction efficiency}\ (\%) = \frac{M \text{ in solution (ppm)} \times \text{water in leaching (ml)}}{100 \times M \text{ in magnet}\ (\%) \times \text{magnet amount in acid mixing (g)}} \quad (6)$$

$$\text{Purity of solution}\% = 100 \times \frac{\sum \text{REM in solution (ppm)}}{\sum M \text{ in solution (ppm)}} \quad (7)$$

Results and Discussion

Characterization of Materials

Chemical compositions of the starting magnet samples are given in Table 3. Although differences in elemental composition are common, a typical NdFeB magnet consists of three phases (Fig. 1): the $Nd_2Fe_{14}B$ grain phase, the less abundant grain boundary phase which is usually found as NdO or Nd_2O_3, and the minor $Nd_1Fe_4B_4$ phase. The XRD patterns of the HG and NC samples show different peak intensities which must have been caused by more intensive ball milling conditions in the case of HG sample. During oxidation, the Nd-rich phase transforms into Nd_2O_3 by reaction (8) while oxidation of $Nd_2Fe_{14}B$ phase occurs as a combination of reactions (9–10). Further oxidation enables the formation of $NdFeO_3$ by reaction (11).

$$2\ NdO + 1/2\ O_{2(g)} \rightarrow Nd_2O_3 \quad (8)$$

$$Nd_2Fe_{14}B + 3/2\ O_{2(g)} \rightarrow Nd_2O_3 + 14\ Fe + B \quad (9)$$

$$2\ Fe + 3/2\ O_{2(g)} \rightarrow Fe_2O_3 \quad (10)$$

$$Fe_2O_3 + Nd_2O_3 \rightarrow 2\ NdFeO_3 \quad (11)$$

The distribution of important metals in the bulk HG sample is illustrated in Fig. 2. Roughly, a region dominated by Fe represents the $Nd_2Fe_{14}B$ domains while a region rather highlighted by high Nd and O concentrations represents the grain boundary phase. Any region with high B concentration indicates the minor $Nd_1Fe_4B_4$ phase. Gd and Pr seem to be concentrated in Nd-rich phase. While Al is mostly associated with the grain phase, it is hard to make such a separation for Dy or Co.

Sulfate mixtures were prepared by 13.5 M (with or without stirring) and 14.5 M acid additions. The XRD result is given in Fig. 1 for the 14.5 M acid addition, but it is comparable for the 13.5 M acid addition. Due to the hydrophilic nature of the sulfates, it was only possible to detect neodymium sulfate heptahydrate and iron (II) sulfate monohydrate (szomolnokite). Formation of ferrous sulfate confirms that the water amount is sufficient to enable reaction (1) instead of (2), but that does not necessarily mean this is also the case for higher acid concentrations.

The DSC-TGA result of dried sulfate mixture prepared by 14.5 M acid addition and 24-h drying is given in Fig. 3. Dehydration of the dried mixture is completed at around 300 °C. Although the DSC pattern reveals only one differentiable endothermic peak at 269 °C, the first derivative of weight change with respect to temperature demonstrates four zones corresponding to a 4-step dehydration of the mixture. Although the sample was dried prior to testing, the small bump between 100 and 150 °C indicates removal of physically bonded water. Simultaneous evaporation of excess water can also contribute to the large weight loss at this stage. The remaining three zones at around 200, 230,

Table 3 Chemical compositions of starting magnets (wt%)

Element	Al	B	Co	Cu	Ga	Nb	Fe	Dy	Gd	Nd	Pr	Tb	Eu	Si	Ni	Total
HG	2.12	0.73	0.51	0.16	0.36	0.25	57.2	6.26	2.25	23.0	6.52	–	–	–	–	99.4
NC	0.48	0.86	1.05	0.15	0.21	–	65.0	1.11	–	22.4	6.79	0.69	0.03	0.44	0.62	99.8

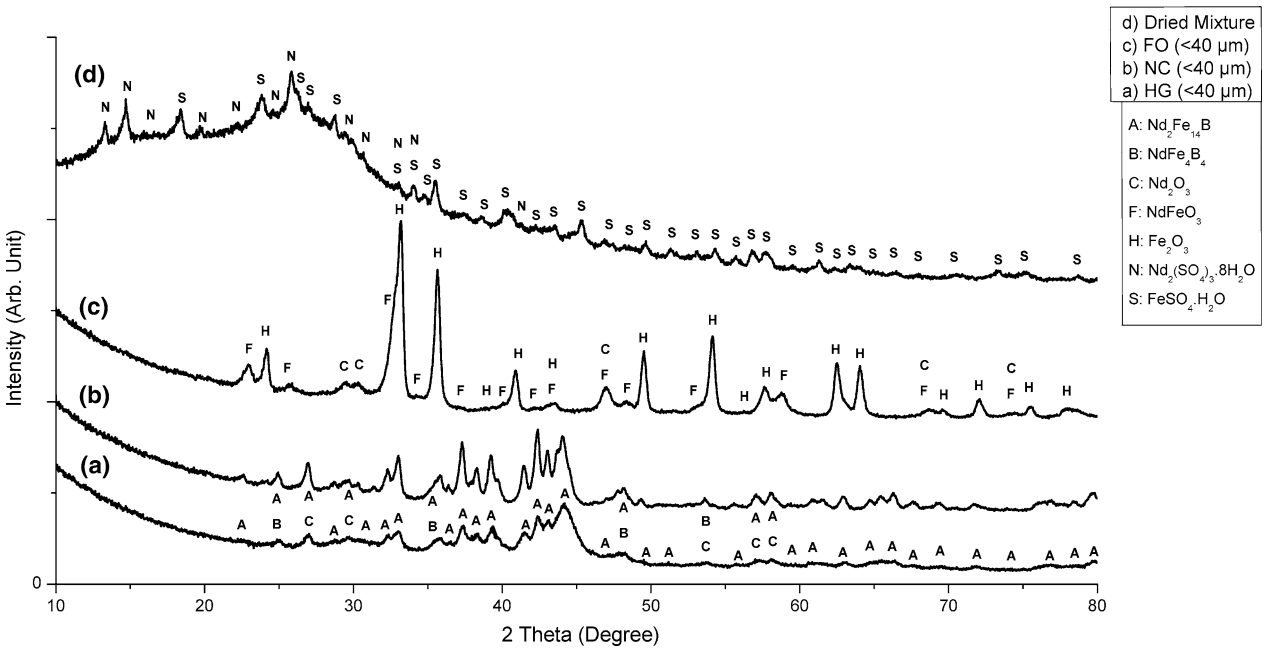

Fig. 1 XRD patterns of starting materials

and 270 °C indicate a three-step dehydration of Nd, Pr, Gd, and Dy sulfate heptahydrates since Fe was originally in the monohydrate form and cannot dehydrate further before 300 °C [47]. The following small endothermic peak at around 325 °C could indicate either dehydration of szomolnokite into anhydrous ferrous sulfate or concurrent oxidation and hydrolysis of the monohydrate to form $Fe_2O(SO_4)_2$ and $FeOHSO_4$ as reported by [51]. The absence of any exothermic or endothermic peak together with no sign of weight loss in the TGA pattern until around 600 °C is in agreement with a combined pathway suggested by [39, 46, 51]. Then, endothermic two-step decomposition of $Fe_2(SO_4)_3$ between 600 and 700 °C resulted in formation of Fe_2O_3 as suggested by [46]. The slight shift to higher temperatures from this previous study must have occurred due to the faster heating rate applied here. Lastly, the small endothermic peak observed at around 872 °C indicates REM oxysulfate formation by reaction (3) and is in agreement with Table 2.

Effect of Acid Concentration

From Fig. 2, it can be concluded that all target metals (e.g., REMs) are distributed over the whole microstructure of the magnet requiring a complete sulfation of the structure. This whole transformation into a paste-like sulfate mixture is then dependent on completion of the metal–acid reactions. Hence, the first attempt was to find sufficient acid concentration that would ensure this aim. In Table 4, the extraction efficiencies of REMs and Fe are given for several acid concentrations at fixed parameters of <40 µm particle size, 24-h drying duration, 110 °C drying temperature, 650 °C roasting temperature, 1-h roasting duration, 25 °C leaching temperature, 24-h leaching duration, and 0.02 g/ml magnet:water ratio. With increasing acid concentration, the extraction efficiencies of REMs and Fe are increasing. This result is incoherent with the DSC-TGA result given in Fig. 3 since 650 °C is quite low for thermal decomposition of water-soluble REM sulfates into water-insoluble REM oxides. Hence the extraction % for REMs should have remained above 90 %. In a similar way, Fe-sulfate is expected to experience a low extent of decomposition to give water-insoluble hematite thereby ensuring less than but close to 100 % extraction at this temperature.

The leach residues obtained after water leaching of 13.5 M (with and without stirring) and 14.5 M acid additions were examined by XRD. As can be seen in Fig. 4, when not stirred, the leach residue of 13.5 M acid addition shares an amorphous noise with the milled magnet with several peaks of Nd_2O_3. Although the stirring action produces a crystalline residue dominated by hematite, still some residual Nd_2O_3 peaks are detectable causing REM losses into residue. By only XRD analysis, it is not possible to differentiate hematite formed by thermal decomposition of $FeSO_4$ from hematite formed by thermal oxidation of the magnet phase in reaction (10). Contrarily, the XRD pattern obtained from 14.5 M acid addition case revealed no phases other than hematite indicating complete transformation and complete subsequent dissolution of REM sulfates with no need of stirring. These results were confirmed

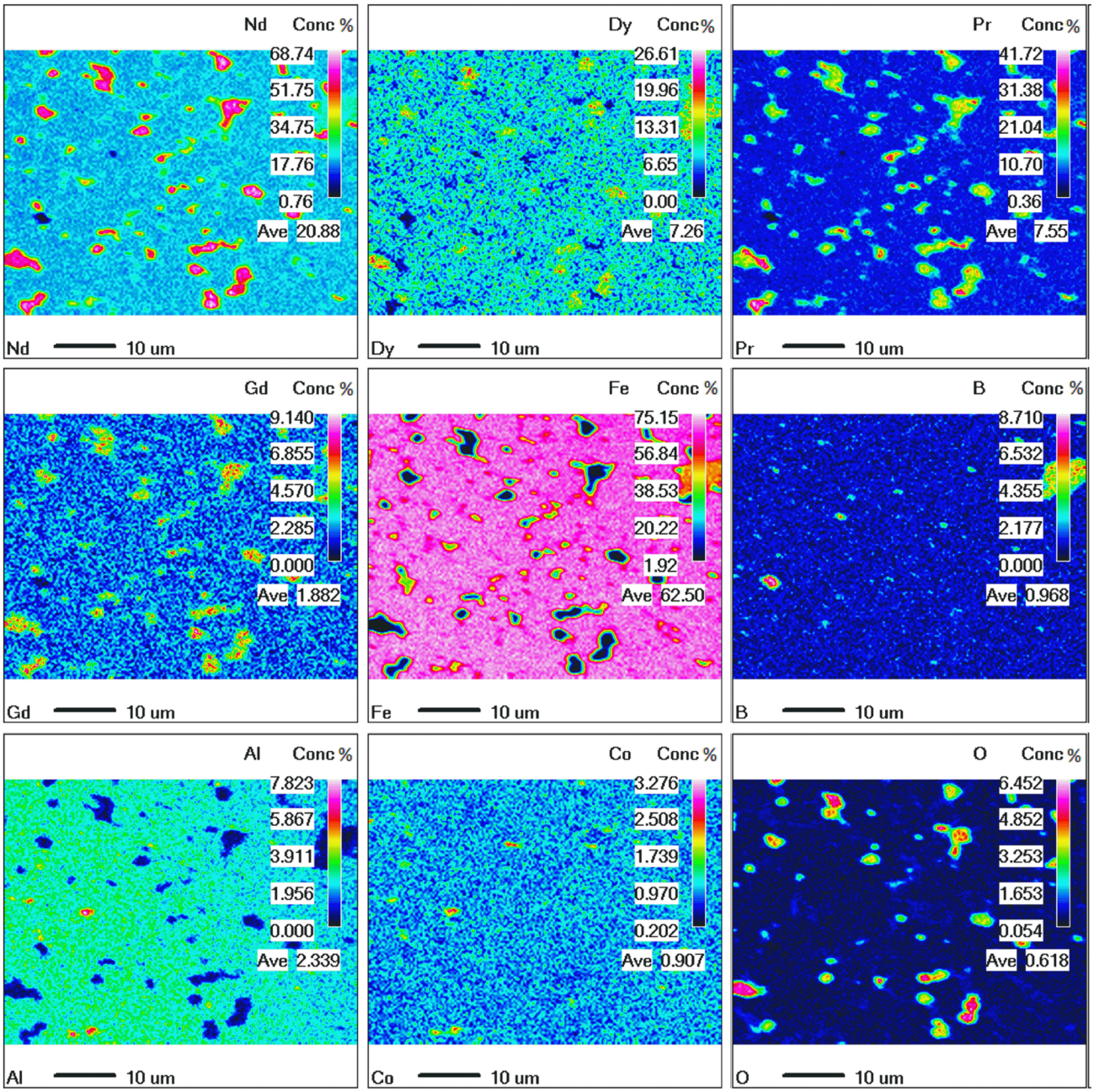

Fig. 2 EPMA mapping for elemental distribution (concentrations are in wt%)

by SEM and EPMA analyses of these residues. In Fig. 5a, b back scattered images of the residues from non-stirred 13.5 and 14.5 M acid additions are given, respectively. Although the starting magnet material was <40 μm in particle size, several tablet-like zones with >40 μm sizes were detected in both cases. Those tablets are formed by a so-called sintering action of the small particles during the acid mixing stage where highly exothermic reactions produce a large amount of local heat fusing particles together. The same coarsening was also observed in the fully oxidized sample after oxidation treatment.

In Fig. 5d, e, several point analyses are taken from contrasting regions of the same residues in Fig. 5a, b, respectively. From the compositions given in Table 5, we conclude that these bright regions in Fig. 5a, d are actually original but oxidized magnet phases enriched with Nd, Dy, Pr, and Gd, while the dark regions are the hematite phase produced by oxidation. Unlike in Fig. 5b, e, the lack of any porous structure in both bright and dark zones of Fig. 5a, d indicates an absence SO_2/SO_3 gas formation suggesting no thermal decomposition during roasting and hence no sulfation of such tablets during acid mixing or drying in the

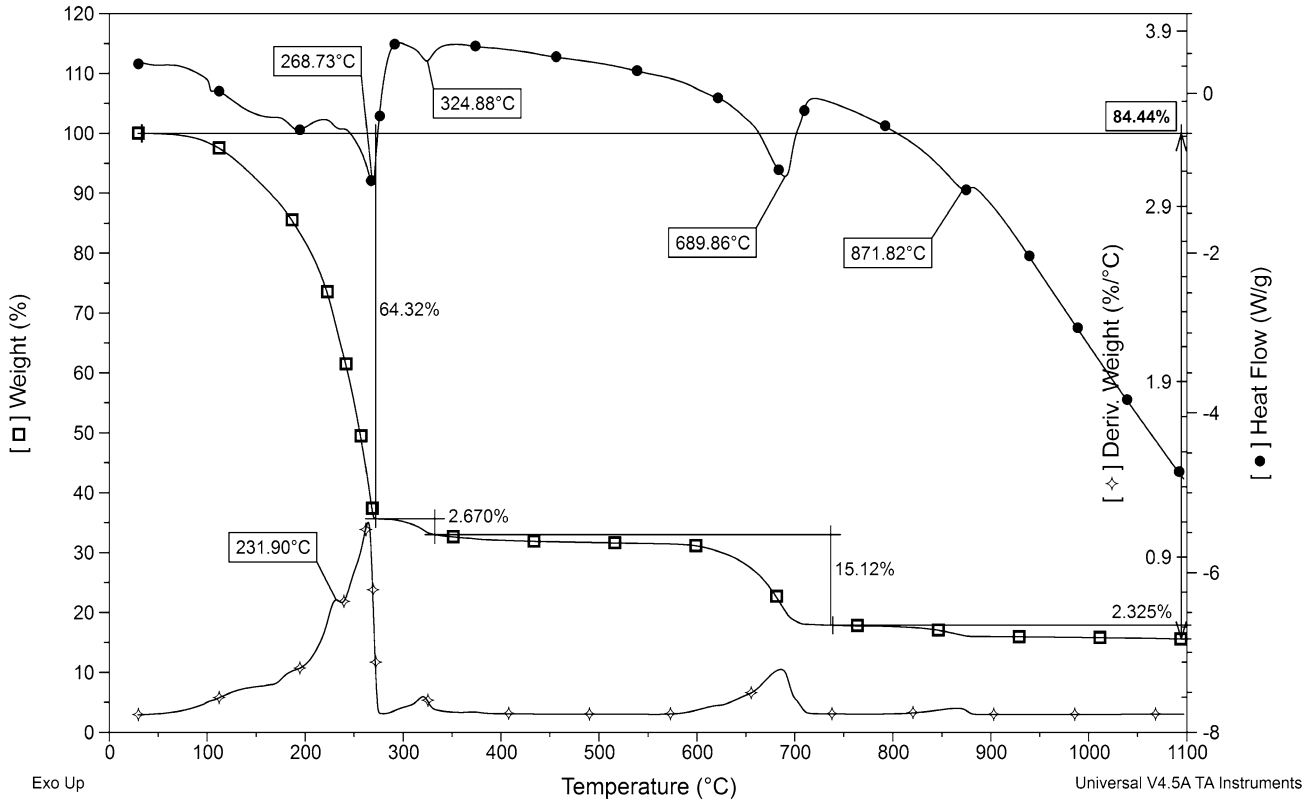

Fig. 3 DSC-TGA analysis of dried mixture (uppermost curve: heat flow; lowermost curve: first derivative of weight % with respect to temperature)

Table 4 Extraction efficiencies of REMs and Fe with different acid concentrations in acid mixing stage (fixed conditions: <40 μm particle size, 24-h drying duration, 110 °C drying temperature, 650 °C roasting temperature, 1-h roasting duration, 25 °C leaching temperature, 24-h leaching duration, and 0.02 g/ml magnet:water ratio)

Acid concentration (M)	12	13.5	12	13.5	14.5	16
Stirring	No	No	Yes	Yes	No	No
Element	Extraction (%)					
Nd	43.4	76.3	90.0	90.9	98.6	100
Pr	45.3	71.6	90.6	91.2	99.5	100
Dy	43.7	68.2	87.2	90.7	99.2	100
Gd	21.2	63.0	89.6	91.2	100.0	100
Fe	41.0	61.5	64.2	72.2	88.9	90.0

first place. Although the same sintering problem can be seen in Fig. 5b for the 14.5 M acid addition case, the acid amount was high enough to almost completely react with such tablets creating a porous structure and allowing ~99 % extractions of all REMs into water. The point analyses given for Fig. 5e indicate negligible (≤0.5 %) REM losses into hematite. The complete recoveries of these metals with 16 M concentration implies that the remaining ~1 % extraction losses in 14.5 M acid addition case are most likely due to residual unreacted zones.

Effect of Drying Duration and Particle Size

After acid mixing, the subsequent drying is to allow sufficient time for metal–acid reactions to be completed, and the supplied heat is for the enhancement of sulfation reaction kinetics. The effect of drying duration on extraction efficiencies of metals is given in Table 6 for fixed conditions of <40 μm particle size, 750 °C roasting temperature, 1-h roasting duration, 25 °C leaching temperature, 24-h leaching duration, and 0.02 g/ml magnet:water ratio. It is clear that the drying duration can be shortened to 6 h with still achieving more than 95 wt% extraction of REMs. Even shorter durations are also possible but with probably increasing losses of these metals. Although only 110 °C was studied here, higher temperatures (i.e., 200 °C) can also be applied to accelerate reactions (1) and/or (2) in shorter drying durations.

Another important parameter for complete sulfation of the magnet sample is its particle size. The bigger the particle size, the harder it is for the acid to reach the core and completely react with the metals inside the magnet. Also,

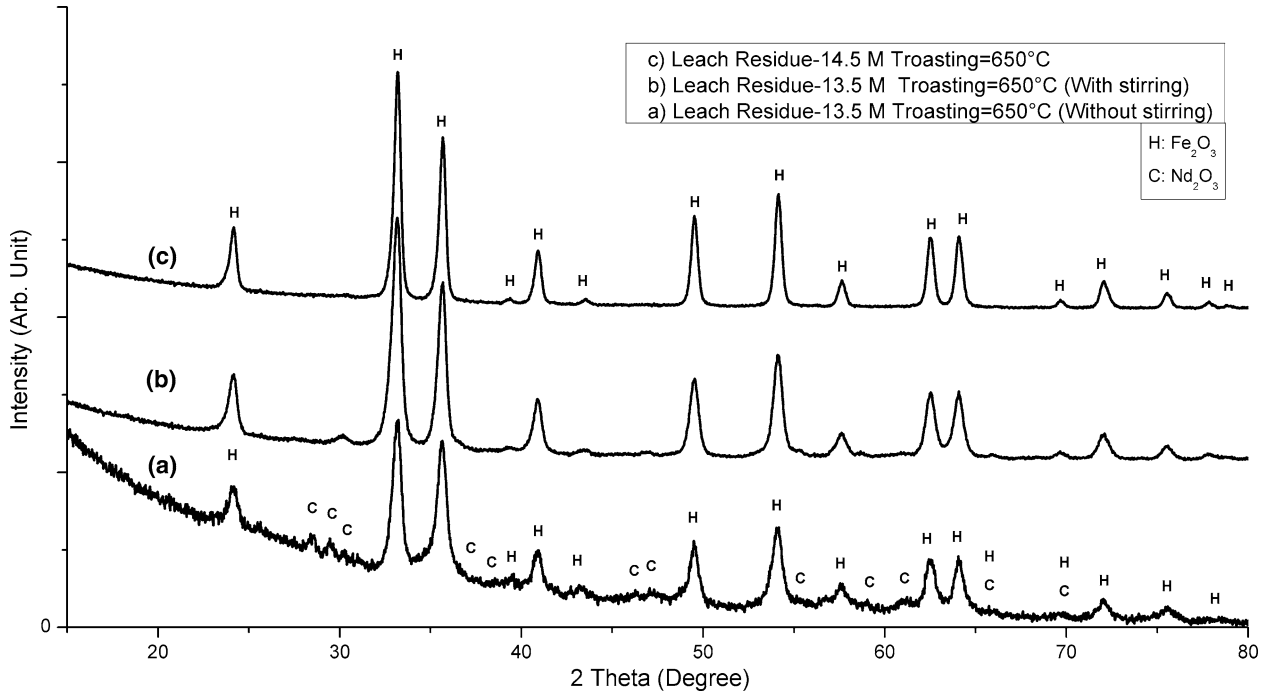

Fig. 4 XRD patterns of leach residues from 13.5 and 14.5 M acid concentration tests

the sintering action during acid mixing will provide larger tablets that will make complete sulfation even harder. As can be seen in Table 6, for 14.5 M acid concentration, the extraction efficiencies are decreasing significantly by around 10–15 % for <200 μm sample. It is worth to note that Dy is affected the most in this case. The reason for this could be its equal distribution in all phases (Fig. 2) which increases the chance of its entrapment in the hematite matrix. Also, Dy is the heaviest REM of those present with the lowest mobility. This might have prolonged its sulfation reactions or its efficient leaching by water. A similar behavior is observed for the next heaviest REM, i.e., Gd, although it is mostly associated with the Nd-rich phase. Nonetheless, a slightly higher acid concentration can recover the extraction efficiencies back to 95 % or more for all REMs at all studied particle sizes. Trace extraction efficiencies of Fe are due to sufficiently high roasting temperature that enabled complete transformation to hematite. If there is any, residual metallic Fe will simply oxidize during roasting to again form insoluble hematite. Among several possibilities giving more than 95 % extraction efficiencies of REMs, either (i) 24-h drying duration, 14.5 M acid concentration, and <40 μm particle size; or (ii) 24-h drying duration, 16 M acid concentration, and <125 μm particle size can be selected as the optimal combinations for acid mixing providing >98 % REM extraction. In this study, further tests were done by selecting conditions (i) so as to consume less acid.

Effect of Roasting Temperature

Roasting conditions are crucial for the decomposition behavior of impurity and REM sulfates. They directly control both the extraction performances of REMs and the selectivity of the process. The extraction efficiencies of metals and terminal pH of the solutions are given in Fig. 6 for different roasting temperatures. Along with the optimal acid mixing parameters, the other constant parameters were 1-h roasting duration, 25 °C leaching temperature, 24-h leaching duration, and 0.02 g/ml magnet:water ratio.

Between 650 and 750 °C, the extraction efficiencies of all REMs are ~100 %, which then start to decrease first slightly toward 90 % at 800 °C and even more significantly at 850 °C. This gradual decrease in the extraction efficiencies is caused by the formation of water-insoluble oxysulfates. As in Fig. 7, the calcine after 650 °C roasting consists of a mixture of anhydrous trivalent sulfates of Nd and Fe and hematite, which is in agreement with the DSC-TGA result in Fig. 3. After roasting at 750 °C, the ferrous sulfate decomposes completely to give hematite, while the sulfates of REMs are still intact in the calcine. The leach residues of these two roasted samples contain only hematite since ferrous and REM sulfates are completely soluble in water. The acidity of the solution is directly affected by the extraction behaviors of Fe and REMs. Fe has the highest concentration in the magnet followed by REMs combined (Table 3). The solution is highly acidic after

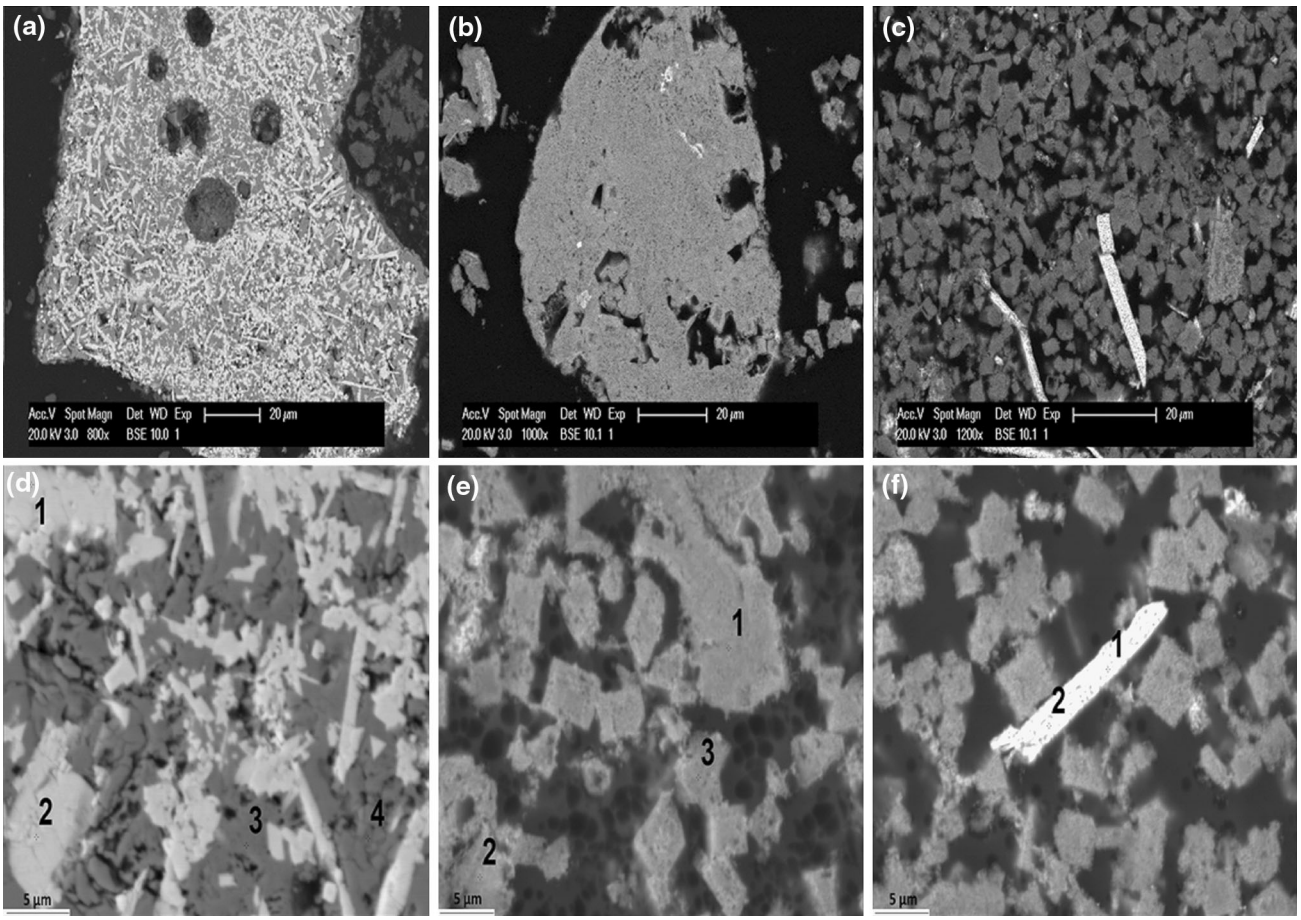

Fig. 5 SEM and EPMA images of leach residues obtained from non-stirred. **a**, **d** 13.5 M and **b**, **e** 14.5 M acid additions after 650 °C, and **c**, **f** 14.5 M acid addition after 850 °C roasting for 1 h

Table 5 Point analysis results from leach residues in Fig. 5d–f

Point No	Nd	Pr	Dy	Gd	O	Fe	S	Co	Nb	Al
d-1	38.1	11.4	13.8	4.02	24.5	3.28	0.02	0.06	0.64	0.24
d-2	38.9	11.5	13.9	3.86	24.8	1.57	0.02	0.38	0.70	0.22
d-3	1.22	0.27	0.15	0	32.4	65.4	0.03	0.13	0.35	0.03
d-4	1.76	0.54	0.40	0.05	30.5	65.0	0.01	0.43	0.48	0.88
e-1	0.21	0	0.19	0	26.0	71.4	0.14	0.29	0.60	1.05
e-2	0.19	0.06	0.43	0.01	23.0	74.9	0.20	0.34	0.42	0.38
e-3	0.16	0.03	0.30	0.05	27.5	70.2	0.13	0.27	0.59	0.63
f-1	31.9	8.34	19.9	4.34	22.4	5.32	6.98	0.07	0.73	0.06
f-2	35.4	9.15	19.7	5.15	17.7	4.53	7.39	0.38	0.54	0.02

roasting at 650 °C (terminal pH 1.5) due to high extraction and dissolution of REMs and more importantly Fe. The sharp increase in the pH between 700 and 750 °C roasting temperatures confirms that all of the dissolved Fe^{3+} ions from $Fe_2(SO_4)_3$ in the case of roasting at 650 °C are now completely absent in the solution produced by roasting at 750 °C .

When roasting temperature is further increased to 850 °C, a new phase appears in the XRD patterns of the respective calcine and the residue in Fig. 7. The initial slight drop in the REM extraction efficiencies at 800 °C indicates that REM oxysulfates form in minor amounts at this temperature, and their amount in the calcine (hence in the residue) increases with the increasing roasting temperature. SEM and

Table 6 Extraction efficiencies of REMs and Fe with different drying durations and magnet particle sizes (fixed conditions: 750 °C roasting temperature, 1-h roasting duration, 25 °C leaching temperature, 24-h leaching duration, and 0.02 g/ml magnet:water ratio)

Duration (h)	6	12	24	24	24	24	24
Particle size (μm)	<40	<40	<40	<125	<200	<125	<200
Acid concentration (M)	14.5	14.5	14.5	14.5	14.5	16	16
Element	Extraction (%)						
Nd	96.9	97.0	98.5	97.4	91.7	99.0	98.7
Pr	98.6	98.8	99.5	96.5	91.7	98.7	98.3
Dy	96.3	98.5	99.1	92.2	87.0	96.0	94.7
Gd	96.4	97.6	99.9	93.7	89.6	96.1	95.1
Fe	0.03	0.02	0.02	0.01	0.01	0.01	0.01

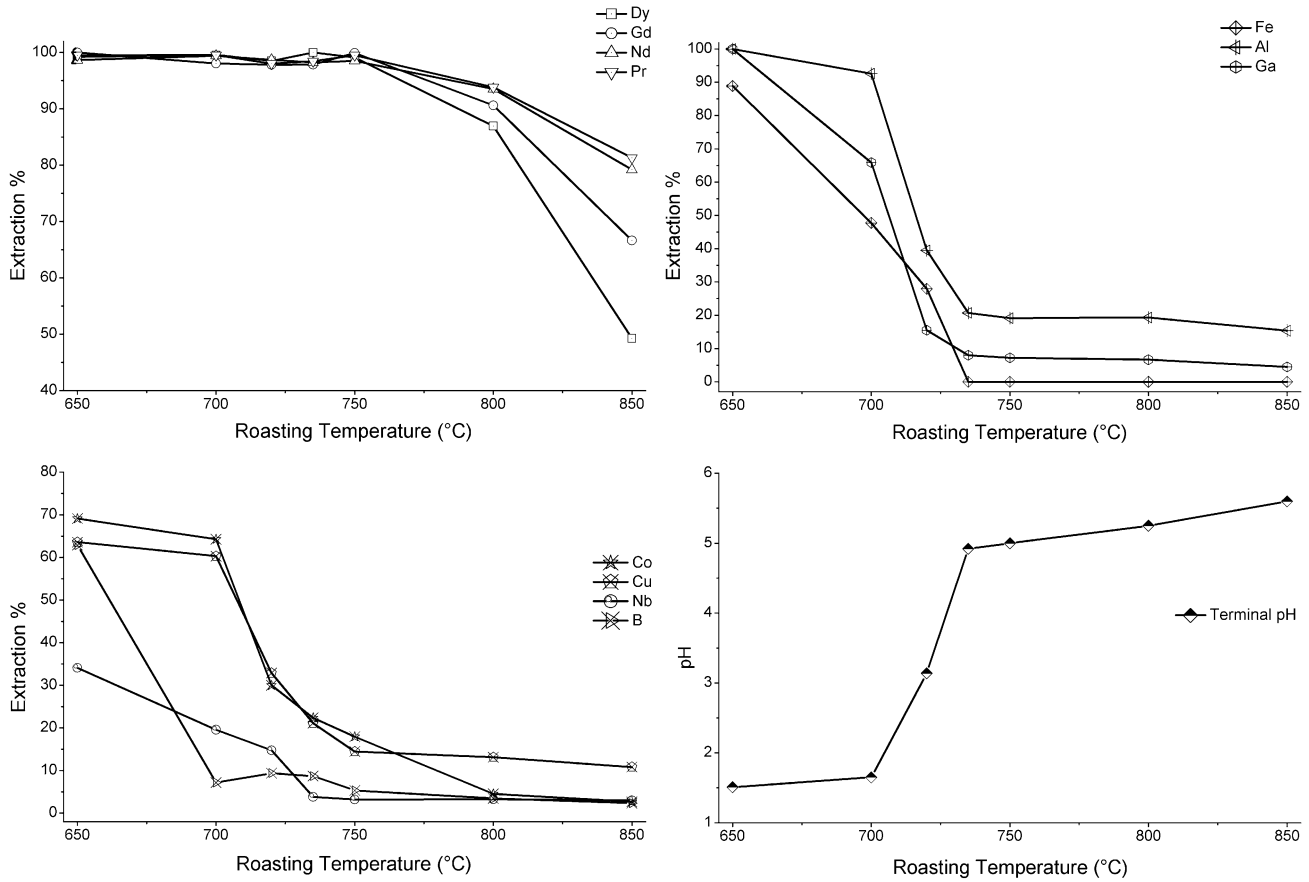

Fig. 6 Effect of roasting temperature on terminal pH of the solution and extraction % of metals (fixed conditions: 1-h roasting duration, 25 °C leaching temperature, 24-h leaching duration, and 0.02 g/ml magnet: water ratio)

EPMA analyses results in Fig. 5c, f and Table 5 reveal that these oxysulfate phases usually occur in a porous needle-like structure and contain a significant amount of REMs causing decreases in their extraction efficiencies. Around 7 wt%, sulfur existence corresponds to the theoretical value for a $Nd_2O_2(SO_4)$ compound. The relatively small increase in the pH between 800 and 850 °C roasting conditions also indicates the decrease in the total concentration of REM ions in the solution. Overall, the thermal sensitivity of REM sulfates could be listed as Nd ~ Pr < Gd < Dy, and 850 °C is the maximum roasting temperature to study within 1-h roasting duration.

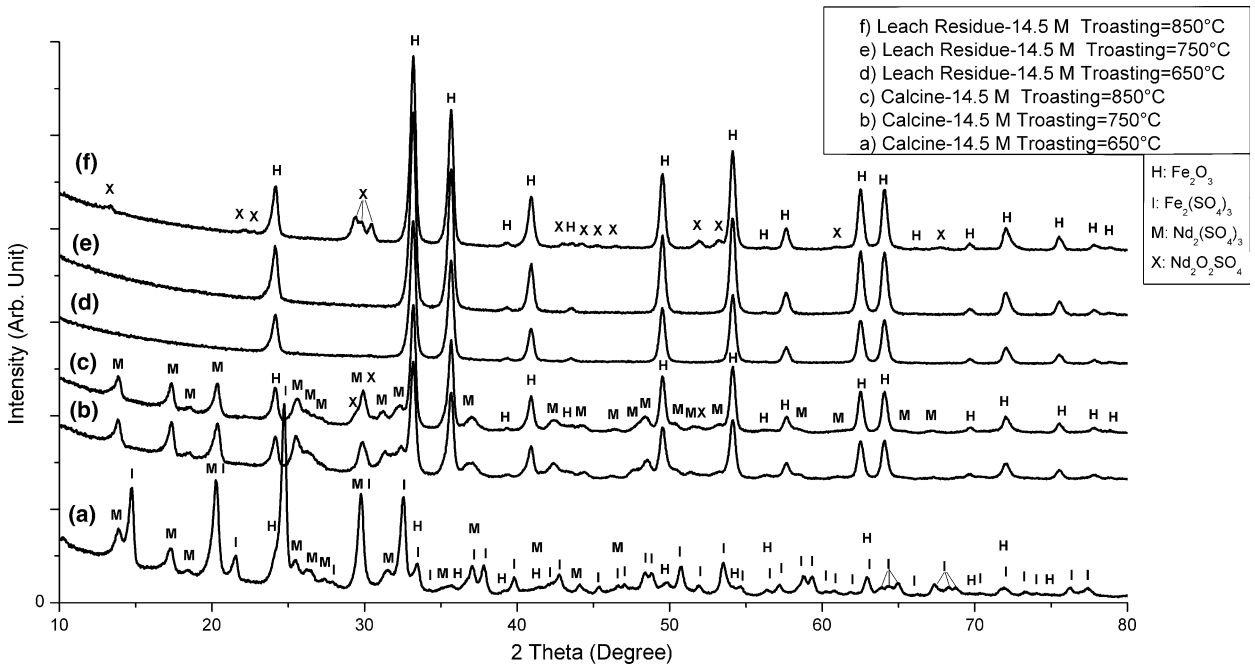

Fig. 7 XRD patterns of calcines and leach residues at different roasting temperatures

The decomposition behaviors of other impurities are also quite important for the purity of the leachate. In Fig. 6, except for Al and Ga, all impurity sulfates are already experiencing decomposition to a certain extent when roasting at 650 °C. It is also possible that metals like Nb are extracted to a smaller extent than the others due to their resistive nature against concentrated sulfuric acid attack. Applying higher roasting temperatures within the same 1-h duration fosters their thermal decomposition reaction. The sharp decrease in extraction efficiencies of all impurity metals between 700 and 750 °C are mostly in agreement with the decomposition ranges given in Table 2. After roasting at 750 °C, only Al, Co, and Cu have more than 10 % extraction efficiencies while the rest are extracted by <5 %. Increasing the roasting temperature to 850 °C, almost completely removes these metals, while only for Al and Cu still longer durations or higher temperatures are required. Matori et al. reported that Al sulfate might survive temperatures up to 900 °C without complete decomposition [53], but Cu sulfate must have completely decomposed to at least its oxysulfate form (Table 2). This minor dissolution of Cu is due to partial solubility of its oxysulfate. Based on these results, either 750 or 800 °C can be selected as the optimal roasting temperature with 1-h roasting duration.

Effect of Roasting Duration

In order to observe the effect of roasting kinetics on extraction efficiencies, several experiments were conducted at 750 and 800 °C roasting temperatures at constant parameters of 25 °C leaching temperature, 24-h leaching duration, and 0.02 g/ml magnet:water ratio. The extraction efficiencies for all metals are given in Fig. 8. When the roasting temperature is 750 °C, REMs are extracted by ~100 % whereas in the case of 800 °C, 95 % or more extraction efficiencies are only possible at 15 min roasting duration. The longer durations seem to enable oxysulfate formation, especially for Dy, thereby decreasing its extraction while for the other REMs it is still possible to preserve ~95 % extractions. The effect of duration seems to have more pronounced results on the impurities. While it takes only 30 min to remove more than 80 % of all impurities at 800 °C, at least 60 min is required for the same purpose at 750 °C. However, the decrease in Dy extraction to 90 % in the former case is less attractive.

Effect of Leaching Conditions

After optimization of the roasting conditions at 750 °C and 1 h, a first attempt was made for shortening the leaching duration at constant parameters of 25 °C leaching temperature and 0.02 g/ml magnet:water ratio. Since water solubility of REM sulfates is decreasing with increasing temperature (Table 1), higher leaching temperatures can only cause a decrease in REM extractions. In Table 7, even at room temperature, leaching occurs fast enough to give 95 % or more extraction for REMs in only 1 h. In contrast, the extraction behavior of the impurity metals is insensitive

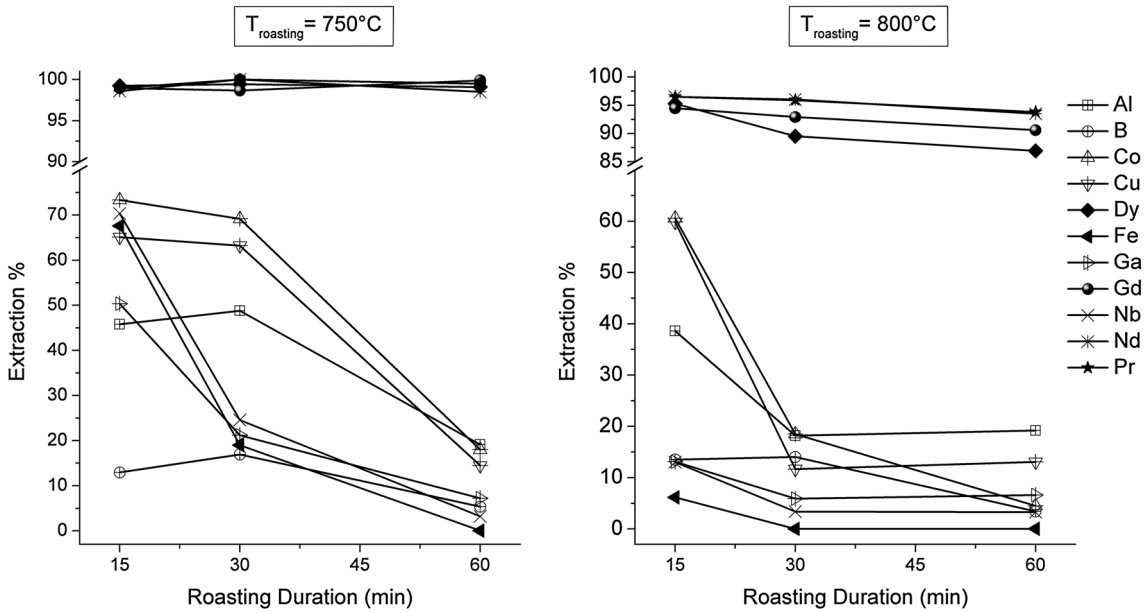

Fig. 8 Effect of roasting duration on extraction efficiencies of metals after roasting at **a** 750 °C and **b** 800 °C (fixed conditions: 25 °C leaching temperature, 24-h leaching duration, and 0.02 g/ml magnet: water ratio)

Table 7 Effect of leaching duration on metal extraction efficiencies

Roasting duration (h)	1	1	1	1	1	2
Leaching duration (h)	24	6	1	1	1	1
Magnet:water ratio (g/ml)	0.02	0.02	0.02	0.06	0.10	0.06
Element	Extraction (%)					
Dy	99.1	98.3	94.6	96.2	85.8	95.3
Gd	99.9	99.7	96.3	98.3	92.6	98.6
Nd	98.5	100.0	98.2	100.0	83.1	99.9
Pr	99.5	100.0	97.5	99.6	87.0	100.0
Fe	0.02	0.05	0.04	12.6	4.48	0.01
Al	19.1	18.5	17.9	20.3	16.6	10.4
B	5.34	25.3	23.6	15.6	21.5	12.9
Co	18.0	26.9	23.4	22.3	23.6	11.5
Cu	14.5	13.9	13.1	31.0	20.7	10.4
Ga	7.23	7.11	6.71	10.5	5.21	5.11
Nb	3.21	3.03	3.00	16.4	8.29	1.64

against leaching duration except for B. Around 20 % decrease in extraction efficiency for B after 24-h leaching can be caused by complexation with hematite. Probably, adsorption of light boron ions by the porous hematite during such prolonged durations can be responsible for this decrease.

In order to increase the output of the process, the magnet:water ratio was increased to 0.06 and 0.10 g/ml ratios at constant parameters of 25 °C leaching temperature and 1-h leaching duration. The obtained results are also given in Table 7. In the extraction efficiencies of all REMs, there are slight increases in the 0.06 ratio case, which is followed by drastic declines toward 80 % for the 0.10 ratio. Meanwhile, for most of the impurity metals, including Fe, this maximal extraction at 0.06 ratio is more clearly visible. The initial increments in the extractions for the 0.06 ratio are simply due to the increased amount of calcine in the experiments requiring longer roasting durations. As can be seen in Table 7, extending the roasting duration to 2 h completely restores the impurity extractions back to the usual low values. Even with this extension, it is still possible to preserve almost complete extractions of REMs. Since the sulfates of impurity metals are experiencing decomposition reactions at relatively lower temperatures than those of REMs, their extraction behavior is affected more. On the other hand, the variations between impurity extractions are caused by the relative stabilities of their sulfate forms, and their initial concentrations in the magnet sample. The decreases in extraction performance of all metals in the 0.10 ratio case is due to the significantly decreased amount of available water, which resulted in two possible causes. Either the low amount of water could not effectively dissolve the metal sulfates within the given leaching duration, or all these sulfates have reached their solubility limits in Table 1 and partially precipitated as the respective sulfate crystals. Overall, it is possible to increase the magnet:water ratio up to 0.06 under the given conditions but with at least 2-h roasting duration

so as to fully restore the impurity extractions back to minimal values.

Optimal Conditions

After these experiments, several combinations offered more than 95 % extraction efficiencies of REMs and very high selectivity against all impurities (especially Fe). Among them, two sets of optimal conditions were selected: (A) 2-h roasting duration and 0.06 g/ml magnet:water ratio; and (B) 1-h roasting duration and 0.02 g/ml magnet:water ratio both with fixed conditions of <40 μm particle size, 24-h drying duration, 110 °C drying temperature, 750 °C roasting temperature, 25 °C leaching temperature, and 1-h leaching duration. The compositions and purities of the solutions obtained under these conditions are given in Table 8. Additionally, the composition of the residue obtained from the conditions in (B) is listed in the same table. The whole process is summarized as a flow sheet in Fig. 9 together with respective optimal conditions given for set (B).

Applicability on Different Source Materials

In order to test the applicability of this study on different magnet compositions and forms, additional tests were performed on fully oxidized HG (FO) and nickel-coated (NC) magnet samples. For all these experiments, the optimal conditions (B) given for HG sample were used. Since $NdFeO_3$ is resistant against acid attacks, the efficiency of 14.5 M acid concentration was questionable. However, as in Table 9, this concentration gives high extractions for REMs with very good selectivity against impurities. It should be noted that this sample was also stirred during the acid mixing stage due to coarsening of particles after oxidation treatment. Otherwise, it is very well possible that much lower REM extraction performance would have been obtained as in the case of HG sample with low acid concentrations (12 or 13.5 M).

The only difference between HG and NC samples is the elemental composition given in Table 3. As can be seen in Table 9, Nd, Pr, and Dy are once again extracted at 95 wt% or more, regardless of their compositional changes. Tb and Eu, despite of their low initial concentrations, follow the same trend, and this is in agreement with their decomposition behaviors. Since sulfate of nickel is thermodynamically less stable than that of cobalt, Co extraction is higher than Ni. However, Co is now extracted more than that observed for the HG sample under the same conditions. That is probably due to its concentration being twice as high as that in the original magnet requiring enhanced decomposition kinetics. Hence, it is certainly possible to decrease both Co and Ni extractions to lower values by adjusting the roasting temperature to slightly higher levels or by simply extending the duration of roasting.

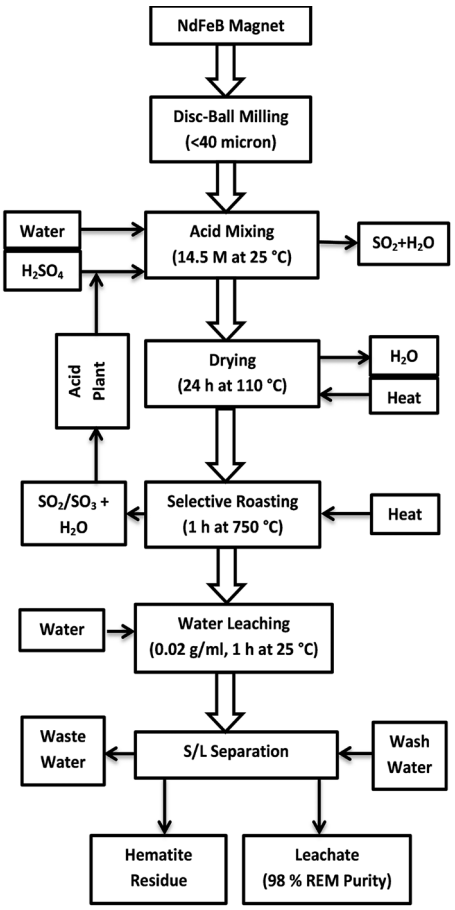

Fig. 9 Process flow sheet containing optimal conditions (B)

Table 8 Compositions of two solutions and a residue obtained from two sets of optimal conditions

Conditions	Element	Nd	Pr	Dy	Gd	Fe	Al	Co	B	Cu	Ga	Nb	Purity (%)
(A)	In solution (ppm)	13692	3885	3555	1322	3.4	131	35	56	10	11	2.4	98.9
(B)	In solution (ppm)	4559	1283	1195	437	4.6	77	24	35	4.2	4.9	1.5	98.0
	In residue (wt%)	0.44	0.14	0.35	0.10	65.9	1.94	0.45	ND	0.16	0.39	0.28	–

Table 9 Extraction results for fully oxidized and nickel-coated magnets

Elements	Extraction (%)										
	Nd	Pr	Dy	Gd	Fe	Al	Co	B	Cu	Ga	Nb
FO	98.7	99.1	94.4	95.5	0.02	7.71	11.3	28.2	7.07	3.62	1.86
Elements	Nd	Pr	Dy	Tb	Eu	Fe	Ni	Co	B	Si	Al
NC	98.9	98.8	94.5	98.2	97.0	0.03	27.9	39.2	10.4	13.4	14.3

Conclusions

The success of this recycling route depends on three accomplishments: (a) completion of sulfation reactions throughout the magnet sample, (b) completion of thermal decomposition reactions of Fe and other impurities, and (c) prevention of any REM oxysulfate formation. By simple adjustments on the conditions of acid mixing–drying, roasting, and leaching steps, several possibilities offered 95–100 wt% extractions of REMs and ~0 wt% extraction of Fe. It is clear from Table 8 that 98 wt% or more purity of the REM concentration is obtainable from a composition given for the magnet. Knowing that Fe is the major impurity metal and will behave in the same way regardless of its concentration, almost complete removal of Fe is granted for any magnet composition by applying the method proposed in this study. Even though impurities other than Fe (e.g., Al, Co, or Ni) still have relatively noticeable extractions, these high-purity levels are obtainable. That is because of their maximum 3–5 % individual contents in NdFeB magnets. Along with their low extraction efficiencies due to selective roasting, low-impurity concentrations in the leachate are granted. Such a solution then can be treated with SX to directly separate and produce REMs with no need of pretreatments for impurity removal. Alternatively, a suitable precipitation–calcination method can produce a REM oxide blend with the same high-purity levels. An obtained blend with such purity can be directly forwarded to an appropriate electrolysis process for production of pure REMs. On the other hand, a hematite-dominated residue with a composition given in Table 8 can be utilized as a source material by the steelmaking or pigment industry. Most importantly, the majority of acid is consumed by impurities (especially Fe) and is recyclable due to the thermal decomposition of impurity-sulfates into the respective oxides. SO_2/SO_3 gas is a by-product of these reactions and is an ingredient for H_2SO_4 production.

Acknowledgments The research leading to these results has received funding from the European Community's Seventh Framework Programme ([FP7/2007-2013]) under grant agreement no. 607411 (MC-ITN EREAN: European Rare Earth Magnet Recycling Network). This publication reflects only the authors' view, exempting the Community from any liability. Project website: http://www.erean.eu. The authors gratefully acknowledge support from the Hercules Foundation (Project ZW09-09). Authors would like to thank Britt Vandenbroeck, Pieter L'hoëst, and Paul Crabbé for their large contribution to sample preparation, ICP-OES, EPMA, and XRF analyses.

References

1. Schüler D, Buchert M, Liu R, Dittrich S, Merz C (2011) Study on rare earths and their recycling. Öko-Institut e.V, Darmstadt
2. Binnemans K, Jones PT, Blanpain B, Van Gerven T, Yang Y, Walton A, Buchert M (2013) Recycling of rare earths: a critical review. J Clean Prod 51:1–22. doi:10.1016/j.jclepro.2012.12.037
3. Yu LQ, Wen YH, Yan M (2004) Effects of Dy and Nb on the magnetic properties and corrosion resistance of sintered NdFeB. J Magn Magn Mater 283:353–356. doi:10.1016/j.jmmm.2004.06.006
4. Le Breton JM, Teillet J (1991) Mössbauer and X-ray study of NdFeB type permanent magnets oxidation: effect of Al and Nb addition. J Magn Magn Mater 101:347–348
5. Skulj I, Evans HE, Harris IR (2007) Oxidation of NdFeB-type magnets modified with additions of Co, Dy, Zr and V. J Mater Sci 43:1324–1333. doi:10.1007/s10853-007-2229-y
6. El-Moneim AA, Gebert A, Uhlemann M, Gutfleisch O, Schultz L (2002) The influence of Co and Ga additions on the corrosion behavior of nanocrystalline NdFeB magnets. Corros Sci 44:1857–1874. doi:10.1016/S0010-938X(01)00163-9
7. Rademaker JH, Kleijn R, Yang Y (2013) Recycling as a strategy against rare earth element criticality: a systemic evaluation of the potential yield of NdFeB magnet recycling. ACS Environ Sci Technol 47:10129–10136
8. Dent PC (2012) Rare earth elements and permanent magnets. J Appl Phys 111:07A721. doi:10.1063/1.3676616
9. Vander Hoogerstraete T, Blanpain B, Van Gerven T, Binnemans K (2014) From NdFeB magnets towards the rare-earth oxides: a recycling process consuming only oxalic acid. RSC Adv. doi:10.1039/C4RA13787F
10. Takeda O, Okabe TH, Umetsu Y (2006) Recovery of neodymium from a mixture of magnet scrap and other scrap. J Alloys Compd 408–412:387–390. doi:10.1016/j.jallcom.2005.04.094
11. Bongaerts JC, Liu J (2013) Production process and recycling of rare earth elements. IMRE J 7:1–9
12. Darcy JW, Bandara HMD, Mishra B, Blanplain B, Apelian D, Emmert MH (2013) Challenges in recycling end-of-life rare earth magnets. J Miner Met Mater Soc 65:1381–1382. doi:10.1007/s11837-013-0783-0
13. Panayotova M, Panayotov V (2012) Review of methods for the rare earth metals recycling. Annu Univ Min Geol St Ivan Rilski Part II, Min Miner Process 55:142–147
14. Harris IR, Williams A, Walton A, Speight J (2012) Magnet recycling. US Patent 2012/0137829A1, 7 Jun 2012

15. Ferron CJ, Henry P (2013) Recycling of rare earth elements. In: London IM, Goode JR, Moldoveanu G, Rayat MS (eds) Proceedings of 52nd conference metallurgist Canadian institute of mining, metallurgy and petroleum, Quebec, Canada, pp 517–531
16. Lee K, Yoo K, Yoon H-S, Kim CJ, Chung KW (2013) Demagnetization followed by remagnetization of waste NdFeB magnet for reuse. Geosyst Eng 16:286–288. doi:10.1080/12269328.2013.858610
17. Anderson CD, Anderson CG, Taylor PR (2013) Survey of recycled rare earths metallurgical processing. Can Metall Q 52:249–256. doi:10.1179/1879139513Y.0000000091
18. Tanaka M, Oki T, Koyama K, Narita H, Oishi T (2013) Chapter 255—recycling of rare earths from scrap. In: Bünzli J-CG, Pecharsky VK (eds) Handbook of physics chemistry rare earths, 43rd ed, pp 159–211
19. Xie F, Zhang TA, Dreisinger D, Doyle F (2014) A critical review on solvent extraction of rare earths from aqueous solutions. Miner Eng 56:10–28. doi:10.1016/j.mineng.2013.10.021
20. Lyman BJW, Palmer GR (1993) Recycling of neodymium iron boron magnet scrap, US Bureau of Mines RI9481
21. Lee C-H, Chen Y-J, Liao C-H, Popuri SR, Tsai S-L, Hung C-E (2013) Selective leaching process for neodymium recovery from scrap Nd-Fe-B magnet. Metall Mater Trans A 44:5825–5833. doi:10.1007/s11661-013-1924-3
22. Rabatho JP, Tongamp W, Takasaki Y, Haga K, Shibayama A (2012) Recovery of Nd and Dy from rare earth magnetic waste sludge by hydrometallurgical process. J Mater Cycles Waste Manag 15:171–178. doi:10.1007/s10163-012-0105-6
23. Yoon H-S, Kim C-J, Lee J, Kim S, Kim J, Lee J (2003) Separation of neodymium from NdFeB permanent magnetic scrap. J Korean Inst Resour Recycl 12:57–63
24. Lee J, Kim W, Jeong J, Yoon IJ (1998) Extraction of neodymium from Nd-Fe-B magnet scraps by sulfuric acid. J Korean Inst Metall Mater 36:967–972
25. Koyama K, Tanaka M (2011) The latest technology trend and resource strategy of rare earths. In: Machida K (ed) The latest technology trend and resource strategy of rare earths. CMC Press, Tokyo, pp 127–131
26. Lyman JW, Palmer GR (2011) Recycling of rare earths and Iron from NdFeB magnet scrap. High Temp Mater Process 11:175–188
27. Tanaka M, Koyama K, Narita H, Oishi T (2012) Recycling valuable metals via hydrometallurgical routes. In: Matsumoto M et al (eds) Design for innovative value towards a sustainable society. Springer, New York, pp 507–512
28. Gupta CK, Krishnamurthy N (2005) Extractive metallurgy of rare earths. CRC Press, Boca Raton, FL
29. Saikkonen PJ (1984) Process for recovering non-ferrous metal values from ores, concentrates, oxidic roasting products or slags. US Patent 4464344, 7 Aug 1984
30. Wendlandt WW, George TD (1961) A differential thermal analysis study of the dehydration of the rare-earth (III) sulphate hydrates. The heats of dehydration. J Inorg Nucl Chem 19:245–250
31. Wendlandt WW (1958) The thermal decomposition of yttrium and the rare earth metal sulphate hydrates. J Inorg Nucl Chem 7:51–54
32. Poston JA, Siriwardane RV, Fisher EP, Miltz AL (2003) Thermal decomposition of the rare earth sulfates of cerium(III), cerium(IV), lanthanum(III) and samarium(III). Appl Surf Sci 214:83–102. doi:10.1016/S0169-4332(03)00358-1
33. Habashi F (1986) Chapter 12: Sulfation of oxides. In: Principles of extractive metallurgy, vol 3: Pyrometallurgy. Gordon and Breach Science Publishers S.A., Langhorne, PA
34. Kaye and Laby Online (1995) 3.2 Properties of inorganic compounds. Tables Phys Chem Constants 16th Ed Version 1.0 (2005)
35. Lide DR (2004) Properties of the elements and inorganic compounds. Handb. Chem. Phys., 85th ed. CRC Press, Boca Raton, FL, pp 1–158
36. Willard HH, Fowler RD (1932) Quantitative separations by the thermal decomposition of anhydrous mixtures of metal sulfates. J Am Chem Soc 54:496–516
37. Patnaik P (2002) Handbook of inorganic chemicals. McGraw-Hill, New York
38. Stern KH (2001) High temperature properties and thermal decomposition of inorganic salts with oxyanions. Part 1. Sulfates. CRC Press, New York, pp 59–78
39. Stern KH, Weise EL (1966) High temperature properties and decomposition of inorganic salts Part 1. Sulfates. National Bureau of Standards, Washington, D.C.
40. Nathans MW, Wendlandt WW (1962) The thermal decomposition of the rare-earth sulphates thermogravimetric and differential thermal analysis studies up to 1400 °C. J Inorg Nucl Chem 24:869–879
41. Wilfong RL, Domingues LP, Fulrong LR (1964) Thermogravimetric analysis of five salts of praseodymium, neodymium, and samarium. J Am Ceram Soc 47:240–241. doi:10.1111/j.1151-2916.1964.tb14403.x
42. Tomaszewicz E, Leniec G, Kaczmarek SM (2010) Re-investigations of thermal decomposition of gadolinium sulfate octahydrate. J Therm Anal Calorim 102:875–881. doi:10.1007/s10973-010-0702-3
43. Tagawa H (1984) Thermal decomposition temperatures of metal sulfates. Thermochim Acta 80:23–33
44. Collins LW, Gibson EK, Wendlandt WW (1974) The composition of the evolved gases from the thermal decomposition of certain metal sulfates. Thermochim Acta 9:15–21
45. Kolta GA, Askar MH (1975) Thermal decomposition of some metal sulphates. Thermochim Acta 11:65–72
46. Siriwardane RV, Poston JA, Fisher EP, Shen M, Miltz AL (1999) Decomposition of the sulfates of copper, iron (II), iron (III), nickel, and zinc : XPS, SEM, DRIFTS, XRD, and TGA study. Appl Surf Sci 152:219–236
47. Swamy MSR, Prasad TP (1983) Kinetics of the thermal decomposition of iron (II) sulphate heptahydrate in air. Thermochim Acta 62:229–236
48. Bristoti A, Kunrath JI, Viccaro PJ (1975) Mössbauer and thermogravimetric analysis of the oxidation pathway in the thermal decomposition of $FeSO_4{\cdot}7H_2O$. J Inorg Nucl Chem 37:1149–1151
49. Neto KS, Garg VK, De Ffsica D (1975) Mossbauer thermal decomposition studies of Fe(II) sulphate. J Inorg Nucl Chem 37:2287–2290
50. Pelovski Y, Petkova V, Nikolov S (1996) Study of the mechanism of the thermochemical decomposition of ferrous sulphate monohydrate. Thermochim Acta 274:273–280
51. Galwey AK, Brown ME (1999) Thermal decomposition of ionic solids. Elsevier B.V, New York
52. Craig BD, Anderson DS (1995) Handbook of corrosion data, 2nd ed. ASM International, Materials Park, OH
53. Matori KA, Wah LC, Hashim M, Ismail I, Zaid MHM (2012) Phase transformations of α-alumina made from waste aluminum via a precipitation technique. Int J Mol Sci 13:16812–16821. doi:10.3390/ijms131216812